Salt concentration effects on mechanical properties of $LiPF_6$/poly(propylene glycol) diacrylate solid electrolyte: Insights from reactive molecular dynamics simulations

Verners, Osvalds; Thijsse, Barend; van Duin, Adri C.T.; Simone, Angelo

DOI
10.1016/j.electacta.2016.10.035

Publication date
2016

Document Version
Final published version

Published in
Electrochimica Acta

Electrochimica Acta

Volume 221, 10 December 2016, Pages 115–123

Salt concentration effects on mechanical properties of $LiPF_6$/poly(propylene glycol) diacrylate solid electrolyte: Insights from reactive molecular dynamics simulations

Osvalds Verners[a], Barend J. Thijsse[b], Adri C.T. van Duin[c], Angelo Simone[a]

Show more

http://dx.doi.org/10.1016/j.electacta.2016.10.035

Open Access funded by European Research Council

Highlights

- correlation between mechanical properties and LiPF6 concentration is observed
- reduced strength and failure strain at increasing LiPF6 concentrations is observed
- correlation between LiPF6 concentration and ion clustering is confirmed

Abstract

Multifunctional composites with load carrying and electrical energy storage capability are relevant for diverse applications. Due to often conflicting requirements for improving both functions, extended knowledge of mechanical material properties is crucial. This study analyzes the mechanical properties of a solid polymer electrolyte material for structural

Electrochimica Acta 221 (2016) 115–123

Contents lists available at ScienceDirect

Electrochimica Acta

journal homepage: www.elsevier.com/locate/electacta

Salt concentration effects on mechanical properties of $LiPF_6$/poly(propylene glycol) diacrylate solid electrolyte: Insights from reactive molecular dynamics simulations

Osvalds Verners [a], Barend J. Thijsse [b], Adri C.T. van Duin [c], Angelo Simone [a]

[a] Faculty of Civil Engineering and Geosciences, Delft University of Technology, P.O. Box 5048, 2600 GA Delft, The Netherlands
[b] Department of Materials Science and Engineering, Delft University of Technology, Mekelweg 2, 2628 CD Delft, The Netherlands
[c] Department of Mechanical and Nuclear Engineering, Pennsylvania State University, 136 Research East Building, University Park PA 16802, USA

ARTICLE INFO

Article history:
Received 25 March 2016
Received in revised form 19 August 2016
Accepted 6 October 2016
Available online 26 October 2016

Keywords:
Solid polymer electrolyte
Molecular dynamics
Viscoelastic properties
Failure properties

ABSTRACT

Multifunctional composites with load carrying and electrical energy storage capability are relevant for diverse applications. Due to often conflicting requirements for improving both functions, extended knowledge of mechanical material properties is crucial. This study analyzes the mechanical properties of a solid polymer electrolyte material for structural battery applications by means of reactive molecular dynamics simulations.

Specifically, conditions for improving load carrying capacity are considered. With the aim of determining optimum salt concentration for mechanical performance, we report the findings on the electrolyte salt effects on the polymer's mechanical properties, including hydrostatic failure behavior. The findings indicate a possibility for stiffness improvement above a threshold concentration value, as well as significant differences in isotropic compression and expansion failure behavior. In isotropic expansion and shear, small failure strength and failure strain reduction at increasing salt concentration is observed. In hydrostatic compression no material failure is observed up to 10 GPa.

As a part of the molecular dynamics potential validation, the observed differences between references and test simulation results for ion transport related properties of a common solid polymer electrolyte have been assessed and discussed.

1. Introduction

The main goal of this study is to gain an atomistic level insight into the macroscopic mechanical properties of a typical solid polymer electrolyte (SPE) derived material – poly(propylene glycol) diacrylate (PPGDA) [1] – for 3-D structural battery fiber coating application. More specifically, we aim to obtain additional knowledge about main electrolyte component concentration effects on the material's mechanical properties.

From earlier experimental studies [2–5] it is known that structural batteries can be considered as a potential multifunctional composite material that could simultaneously function as reduced-cost, leakage-free, reduced-weight energy storage and structural elements of arbitrary shape. Moreover, the possibility of designing such multifunctional electrolytes has already been proven experimentally – both as implemented fiber coatings using poly(ethylene oxide) (PEO) based materials [6] and bulk samples containing PEO with additional thio-ether segments [7]. Due to the significantly reduced ionic conductivities compared to organic liquid electrolytes [8,4], the production of ultrathin conformal coatings is of great importance. To this end, due to its compatible conductivity at room temperature (around 1e-6 S/cm) and thin coating manufacturability, the implementation of PPGDA based coating [1] is considered as an interesting alternative to the commonly used PEO based SPEs which are operated at elevated temperatures [8]. We consider the operability of PPGDA based electrolyte at room temperature as its main advantage in view of structural applications.

For implementation purpose, selecting a suitable design is critical. Considering possible architectures for structural batteries, predominantly two-dimensional (2-D) laminate type implementations have been devised [2,5,4,9]. However, a promising alternative could be the three-dimensional (3-D) type architectures. The motivation for this type of architecture is related to the significant reduction in ionic transport distance [10,11], as well as the possibility of producing 3-D fiber/matrix type structural composites

E-mail addresses: o.verners@tudelft.nl (O. Verners), b.j.thijsse@tudelft.nl (B.J. Thijsse), acv13@psu.edu (A.C.T. van Duin), a.simone@tudelft.nl (A. Simone).

http://dx.doi.org/10.1016/j.electacta.2016.10.035
0013-4686/

[6]. Specifically, the 3-D solid battery architecture consists in the integration of both electrode materials into an inter-penetrating monolithic structure using a thin solid electrolyte layer as the separator. For this study, a 3-D battery architecture is assumed. The assumption implies that the relatively low (1e-6 S/cm) conductivity of SPE is acceptable.

Further, alternative means for improving SPE performance by additional functional components, not considered in this study, have been explored. The effects of specific polymer functional components on PEO based SPE mechanical properties and ionic conductivity have been studied computationally. For poly(styrene-block-ethylene oxide) (SEO) copolymer [12], the increase of the mechanical strength has been attributed to increased Li-C conjugation forces which, in turn, have reduced the ionic conductivity. For the same material, a different study [13] has concluded that conductivity of SEO/salt mixtures increases with increasing molecular weight of the copolymers. The latter behavior is attributed to an increase in inhomogeneous local stress fields which reduce the ability of PEO chains to coordinate with Li cations in low ion mobility regions. Another study [14] has estimated ionic conductivity and strength of PEO sulfonic acid-based SPEs with various contents of the PEO polymer. The results indicate improved ionic conductivity at increased hydration level. By taking into account that hydration simultaneously degrades the strength of material, an optimum level of the PEO polymer content w.r.t. strength and conductivity has been identified. Furthermore, an ionic liquid/PEO based SPE deformation study [15] has revealed inverse correlation between the material's stiffness, strength and conductivity, all expressed as functions of ion concentration dependent crystallinity. However, an experimental study on salt/PEO based electrolytes [16] has reported a positive, salt concentration dependent correlation between the electrolytes conductivity and storage modulus. The above mentioned study [15] also reports a direct anisotropic effect of tension loading on ionic conductivity due to polymer re-alignment and changes in crystal size and proportion. In contrast, another more recent experimental study [17] on PEO/$LiClO_4$ based thin film electrolyte reports equivalent deformation induced enhancement of both tension-parallel/in-plane and tension-normal/out-of-plane conductivity of the material. Apart from highlighting the significance of mechanical loading conditions and the anticipated dependence of the electrolyte's mechanical properties on the ionic dopant, these findings suggest a further comparison with multiaxial, including triaxial, loading cases.

2. Method

2.1. Structures

Crosslinked and non-crosslinked PPGDA polymer structures (Figs. 1 and 2) were created using Molden [18] and LAMMPS [19,20].

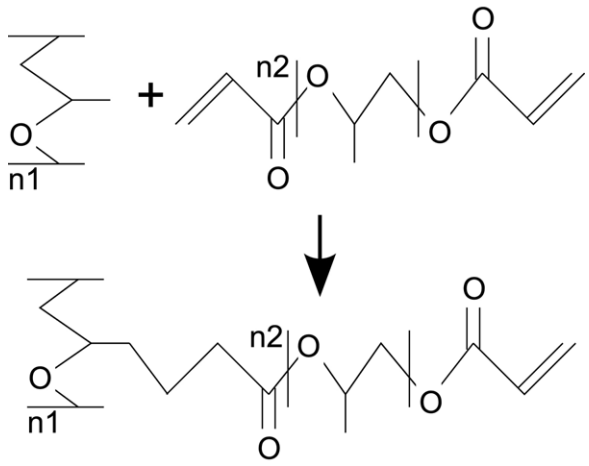

Fig. 1. PPGDA crosslinking reaction.

Orthogonal unit cells of 520 atoms with average dimensions of 17 Å and 18 Å (1 atm, 300K), respectively, were used. $LiPF_6$ molecules at a ratios of Li:EO = 1:16/1:32 (EO = ethylene oxygen atoms) were added to the system during equilibration. The maximum concentration corresponds approximately to that used in a previous experimental study [1]. The unit cell was expanded $2 \times 2 \times 2$ times (size effects are considered in Section 3.2). The structures consist of a mixture of periodic poly(propylene glycol) (PPG) and single unit PPGDA monomers. For crosslinking, the carbon atoms of the methyl group branches of PPG backbone were bonded with the terminal double-bonded carbon atoms of the PPGDA crosslinker monomer acrylate groups (Fig. 1) yielding EO:CO = 3:1 (CO = carbonyl oxygen atoms). Due to the particular crosslink layout, the two directions orthogonal to the periodic backbone direction were deemed most suitable for representing the behavior of an isotropic bulk material. The latter crosslink formation energy had been found to be lower than that of an alternative, backbone carbon bonded, crosslinking (Table 1). Thereby, a periodic crosslinking level of 50 % with respect to the total number of PPG methyl-group C=C crosslinking sites in the system was obtained (Fig. 1b). We would like to point out that, according to an earlier molecular dynamics based study [21], the microscopic polymer stress-strain response of generic polymer melts has been found to be insensitive to heterogeneities due to crosslinking.

Due to availability of extensive experimental data, a chemically similar material – PEO – was used for force field validation purposes. The simulated PEO structure consists of three linear chain polymers of MW = 1e4 g/mol and $LiPF_6$ molecules at a concentration of Li:O = 1:20 yielding a system of 5069 atoms with an average cell dimension of 37 Å (1 atm, 363 K).

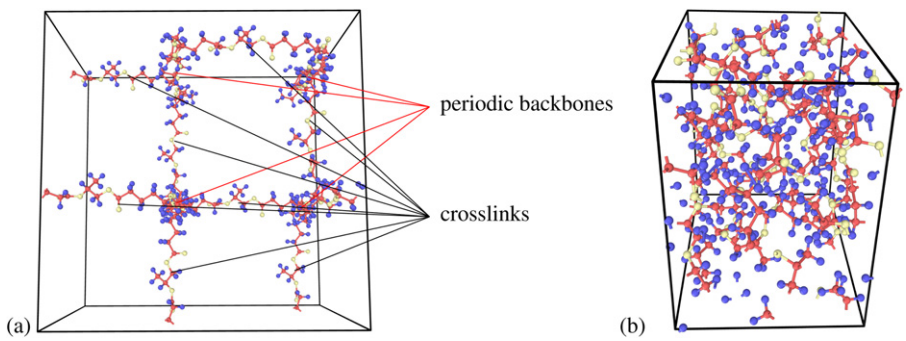

Fig. 2. (a) 0K, 0 atm low density, and (b) 300K, 1atm equilibrated 50 % crosslinked PPGDA polymer 520-atom unit cell (C=red, H=blue, O=yellow).

Table 1
CH_3OCH_3 dissociation, $LiPF_6$ and PPGDA dissociation/crosslinking energies [kcal/mol] (1 kcal/mol=4.184 kJ/mol) and charges (q) [e] (1 e=1.6e-19 C).

structure	ReaxFF	DFT/ReaxFF[a]	DFT	experiment
CH_3OCH_3 C—O dissociation	74.5	-	86.4/82.3[b]	83.2 [58]
$LiPF_6$ dissociation	34	-	105	-
q_{Li} in bonded $LiPF_6$	0.60	-	0.81	-
q_{Li} in dissociated $LiPF_6$	0.49	-	1.00	-
PPGDA branch crosslink	17.4[c]	-	22.8	-
PPGDA backbone crosslink	15.9[c]	-	22.2	-
PPGDA 1-unit dissociation	23.3	110.4	75.8	-
PPGDA 2-unit dissociation	32.6	77.8	76.3/15.4[d]	-
PPGDA periodic dissociation	53.1	80.8	78.2	-

[a] ReaxFF trajectory structures
[b] [57]
[c] MD minimization [59]
[d] reactions without/with H transfer

2.2. Simulation settings

In order to properly account for charge polarization effects during ion migration and study the material bond dissociation failure behavior resulting from bulk deformation, the simulations were performed using the MD package LAMMPS [19] with the reactive empirical force field ReaxFF [22], combined with charge equilibration according to [23] (QEq) in USER-REAXC package [20]. A force field parameter set that describes C/H/P/F/O/S/Li interactions, previously applied to battery related systems [24,25], was used.

The structures were initially energy minimized using a conjugate gradient method (max. force convergence criterion of 1e-6 kcal/mol/Å) combined with quadratic linesearch (max. displacement of 1e-2 Å per outer iteration) [26]. Minimization was stopped if linesearch $\alpha = 0$ was reached. The MD simulations were performed using Verlet type time integration [27] with a 0.25 fs time step. For equilibration at 300K and 1 atm, the Nose-Hoover thermo/barostat was coupled with five chain thermostats [28,26]. LAMMPS equivalent temperature damping constant (100 fs) and pressure damping constants (250 fs) were used, unless noted otherwise, to simulate the isothermal/isobaric (NPT) ensemble. Anisotropic pressure equilibration was applied. For the subsequent isothermal/isochoric (NVT) ensemble equilibration, the Nose-Hoover thermostat was applied. Equilibration was considered as sufficient if the mean potential energy change during a production run would be of order $\sigma_{E_{pot}}$/ns. For stress based dynamic tensile stiffness calculations in the backbone-orthogonal direction, the NPT ensemble with at least two different temperature/pressure damping constant combinations (100/250, 25/25, 25/250 fs) was applied in the stress-free directions of the cell. The strain rate range of [0.08, 8] ns^{-1} was imposed for the dynamic stiffness calculations. The simple shear failure simulations were performed at 12.5 ns^{-1} shear rate. For non-equilibrium dynamic shear viscosity calculation, a shear velocity gradient according to the Muller-Plathe algorithm was applied [29,26].

For validation against DFT results, ionic relaxation calculations were performed using the VASP simulation package [30,31]. For the calculations, the plane augmented wave (PAW) [32,33] implementation was used with the generalized gradient approximation (GGA) PBE exchange-correlation functional [34], DFT D3 van der Waals interaction correction method with Becke-Jonson damping [35] (for condensed phase structures), 1e-4 eV convergence criterion for combined Davidson block iteration [36] / residual minimization method direct inversion in the iterative subspace [37] electronic minimization, and a conjugate gradient energy convergence criterion of 1e-4 eV for the ionic relaxation [38]. For band-structure energy calculations, the linear tetrahedron method with Bloechel corrections [39] and Gauss-like functions [40] with the parameter $\sigma = 0.05$ [38] were used for multiple and less-than-five k-point grids. For k-point grid definitions, the Monkhorst-Pack scheme [41] was used. 400/520 eV plane wave basis set cutoffs were used for constant/variable cell volume calculations. The DFT based atomic charges were calculated using the DDEC [42] method.

2.3. Postprocessing and analysis methods

The reaction coordinate for monomer dissociation energy calculations were defined as the cell dimension change in the direction of deformation for periodic structures and terminal C atom interatomic distance change for non-periodic structures.

Ion self-diffusivities, where PF_6^- ion diffusion was represented by P atoms, were calculated according to the Einstein relation (without linear curve fitting). The ionic conductivity of $LiPF_6$ was calculated by assuming a constant mean ionic charge and converting the known Green-Kubo relation [43] to its corresponding Einstein relation [44,45].. Equilibrium shear viscosities were computed according to the Einstein and Green-Kubo relations [46]. Shear stress relaxation modulus was estimated as a function of the shear stress autocorrelation [47]. The latter methods are known for sensitivity w.r.t. the accuracy of long-range interaction description, which may result in viscosity overestimation [46], and a difficulty for the estimation of stress integral calculation accuracy at long integration times [48,46]. The potential disadvantages, however, are outweighed by the absence of loading rate effects which may be prohibitive for using NEMD based methods with long relaxation time materials due to minimum loading rate restrictions [48,49]. For dynamic stiffness (E) calculations, least-squares curve fitted values were averaged over the linear stress response strain range. Additionally, the dispersion of a curve fit was characterized by the normalized curve fit residual $\mathrm{Res} = (\Sigma[\sigma(E, \varepsilon_{data}) - \sigma_{data}]^2)^{-1/2}/n_{samples}$. Since the latter deformation range involved a transition from high stress, shock loading type response, to a lower stress response, the respective lower stiffness values are expected to approach the low strain rate limit according to experimental predictions [50].

For diffusivity, conductivity, and equilibrium state viscosity calculations, a sliding window averaging algorithm [43] and 10 sampling sets per simulation, each 50 % of full simulation length, were used. We would like to point out that, due to linearly decreasing number of samples vs sampling time, the averaged quantity values up to about 60 % of the maximum sampling time are considered for convergence validation (samples for ionic conductivity estimation provided in Fig. 3). The standard error of averaged quantities was calculated for a 95 % probability interval assuming the normal distribution. For structure visualization, the OVITO software was used [51]. For atomistic level interpretation of the macroscopic property results, atomic structure comparison w.r.t. complexation/coordination structure was performed by applying radial distribution and derived analyses. Specifically,

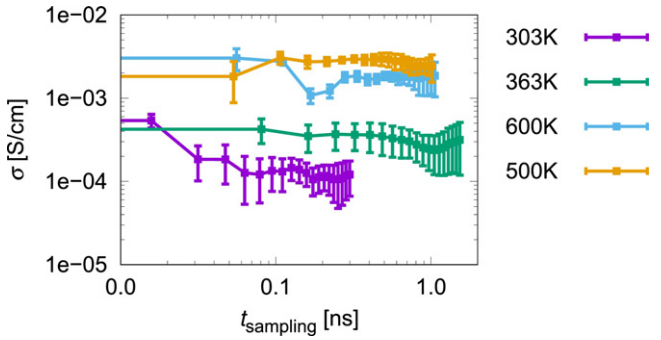

Fig. 3. Sampling time based convergence of $LiPF_6$/PEO ionic conductivity (sliding window averaging applied).

time-averaged radial distribution functions (RDF) $g(r)$ and radial integrals of RDFs (IRDF) Int($g(r)$) were computed using a sampling bin size of 0.1 Å.

Table 2
Physical properties of PEO (300 K, unless noted otherwise).

	ReaxFF	experiment
T_m [°C]	~60[a]	65 [52]
η [mPa·s]	1.7±0.2/11±4[b]	69.1 [60][c]
ρ [g/cm^3]	1.16	1.13 [52][d]

[a] mean of heating/cooling cycles at a rate of 1.2 K/ps
[b] reference densities 1.153/1.165 g/cm^3, resp.
[c] MW=400, 303.15K
[d] MW=1e5, 298K

Table 3
Ionic transport properties of $LiPF_6$/PEO (363K).

	ReaxFF	experiment
D_{Li} [cm^2/s]	2.2±0.3e-7	0.6e-7 [61][a]
D_P [cm^2/s]	1.6±0.1e-7	1.4e-7 [61][a]
σ [S/cm]	2.7±0.9e-4	2e-4 [61][a]

[a] MW=1e5

3. Results and Discussion

3.1. Force field validation

The force field validation was performed by considering both atomistic scale physical properties of poly(propylene glycol) (PPG) and $LiPF_6$ (for comparison with analogous DFT results), and macroscopic scale physical properties of PEO structures (for comparison with experimental results).

Simulation results indicate overall slightly lower crosslink formation energies and CH_3OCH_3 dissociation energy, and significantly reduced PPGDA monomer dissociation energies compared to DFT/experiments (Table 1). The latter energy differences suggest that the actual material failure stresses/strains may be higher than the simulation predictions. Furthermore, for ReaxFF a distinct PPGDA monomer length dependence is observed, which is found to be in qualitative agreement with DFT results (without H transfer for the two-unit monomer). Here we would like to note that no H transfer events were observed for the ReaxFF dissociation trajectories. Last, a slight overestimation of nonbonded interactions is observed both for monomer-monomer and monomer-Li separation trajectories (Fig. 4). Comparison with bond and species statistics from isotropic expansion failure simulations (Section 3.4) indicates that the breakage of all C—$O_{acrylate}$ bonds can be directly linked to the observed cross-linking monomer length dependent failure behavior. Moreover, the absence of H transfer events in all simulations indicates that force field energy barriers for the transfer are higher than those obtained for dissociation of monomers (Table 1).

For PEO, good agreement was found w.r.t. mass density and melting point (Table 2). In contrast to a relatively good agreement with experimental data for PF_6^- ion diffusivity, a significant overestimation of the Li ion self-diffusivity in $LiPF_6$/PEO was found (Table 3). The difference was partially attributed to the estimated dynamic viscosity, which was found to be significantly lower than the experimental values for smaller molecular weight molecules (Table 2), approaching low concentration (5%) water solution level [52]. The latter assumption was founded on the relevance of segmental mobility, characterized by viscosity, in context of ion transport mechanisms (Section 1). The assumption was supported by the observed $Li(PF_6)_n$ complexation structures of ions (Fig. 7) which, in contrast, imply reduced long range Li ion diffusion due to reduced Li-O interactions. The complexation behavior and high Li ion diffusion were attributed to the significantly lower Li-PF_6 dissociation barrier as compared to DFT (Table 2). The difference in dissociation barrier, in turn, was partially attributed to a significant difference in dissociated state Li ion charge (−50% vs DDEC estimate according to Table 1). In view of the latter difference, the observed ionic conductivity underestimation at 600K (PEO dissociation estimated at about 700K) and overestimation at 303K were interpreted as differences in Li ion diffusion mechanisms (Fig. 8), as distinguished between Vogel-Fulcher-Tamman (VFT) and Arrhenius type $\sigma(T)$ relations according to experimental and ReaxFF results, respectively. Further, it should be noted that similar trends with respect to Li vs PF_6^- ion diffusivity (transference related) estimation and $Li(PF_6)_n$ clustering have also been observed in other related MD studies [53,54] thus suggesting that the simulation timescale could be a contributing factor [55,56]. However, an acceptable agreement was observed between ReaxFF and DFT predictions for nonbonded and weakly bonded interactions

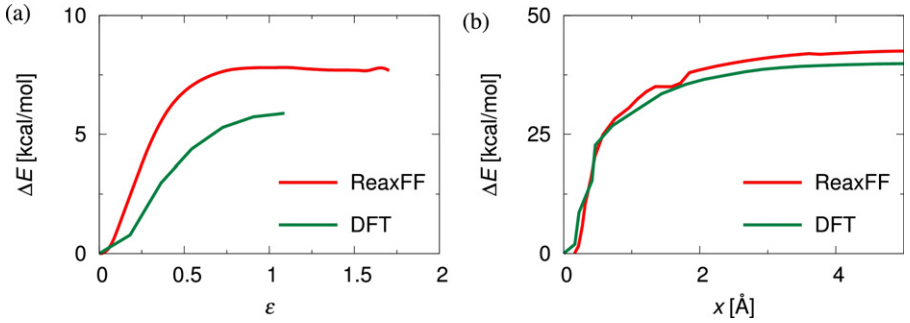

Fig. 4. Comparison of DFT and ReaxFF structure energies (1 kcal/mol=4.184 kJ/mol) for (a) two PPG units at condensed phase density during periodic cell deformation normal to chain-periodic direction (ε = tensile strain), and (b) Li/single-unit PPGDA monomer during weakly bonded Li/monomer separation (reaction coordinate defined as separation distance change).

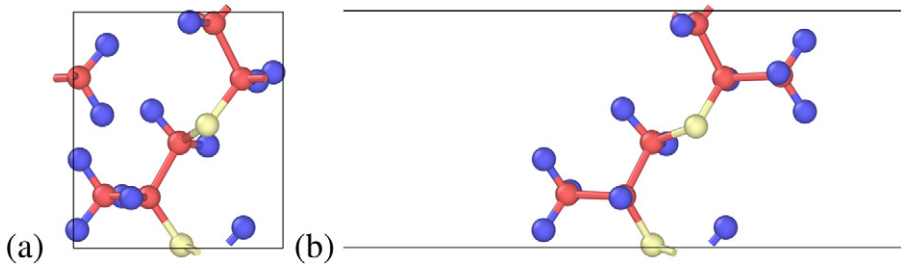

Fig. 5. (a) initial and (b) final configurations of two PPG condensed phase unit cell deformation normal to the periodic chain direction (C=red, H=blue, O=yellow).

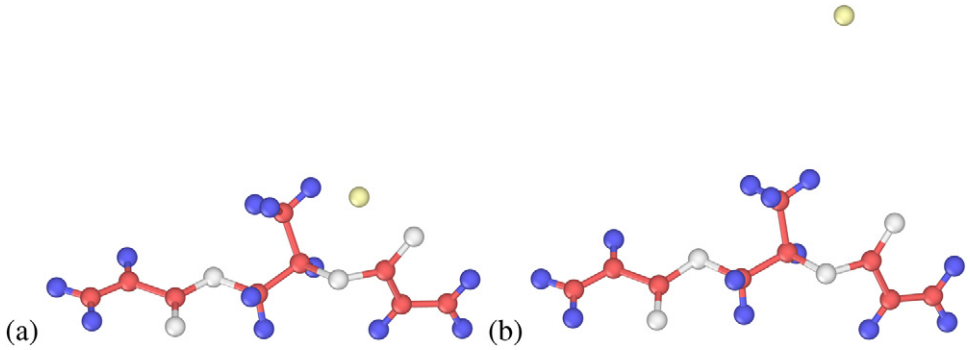

Fig. 6. (a) initial and (b) final configurations of Li separation from a single-unit PPGDA monomer (C=red, H=blue, O=white, Li=yellow).

(Figs. 4, 5 and 6). Subsequently, the ionic transport properties of $LiPF_6$/PPGDA were not considered in this study.

3.2. Crosslinking and size effects

Based on a comparison of dynamic stiffness (E) and its curve fit residual (Res) for structures of different sizes (Fig. 9), size convergence around periodic unit cell expansion levels of $3 \times 3 \times 3$ and $4 \times 4 \times 4$ is estimated. Due to computational expense, however, the expansion level of $2 \times 2 \times 2$ was selected for further study.

According to the stiffness values of the 50 % crosslinked and non-crosslinked structures at strain rate of 8 ns^{-1}, a stiffness increase of approx. 50% and equilibrium viscosity increase of approx. 20× were obtained. Furthermore, irrespective of the system size, the bond-dissociation-free deformation limit in uniaxial tension in the considered strain rate range was found to be close to 300 % for the crosslinked structures (Table 5). Subsequently, by comparing against experimentally obtained stiffness vs crosslink density relation [62], the crosslinking effect on material's elastic properties was considered as moderate and the crosslinked structure was employed for further study.

3.3. $LiPF_6$ concentration and strain rate effects on viscoelastic properties

According to Kohlrausch's law [63], a reduction in ion self-diffusivities/molar conductivities at increasing ion concentrations is expected. This evidently determines optimum ion concentration for maximum electrical conductivity, which corresponds to a trade-off between reduction in ion diffusivity and proportionality to ionic concentration. In contrast, the lowest applied strain rate (0.08 ns^{-1}) allows to predict an increase in the material's stiffness due to $LiPF_6$ concentration (Table 4). The latter trend has been observed experimentally for a different polymer/salt composite [16]. We found the stiffness increase to correlate with the material's shear viscosity (Table 4), indirectly characterized by the initial ($t = 0$) values of shear stress relaxation modulus (Fig. 11), and this motivated a comparison of radial distribution changes

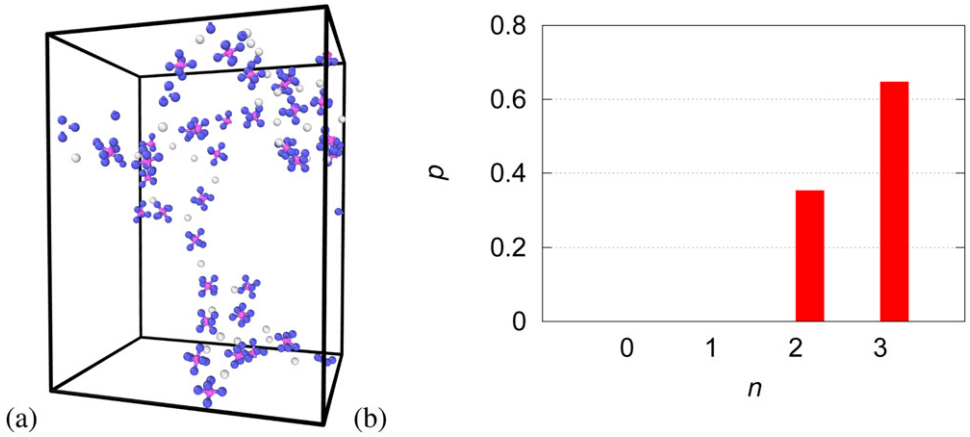

Fig. 7. (a) configuration snapshot (Li=white, F=blue, P=violet), and (b) distribution of Li-$(PF_6)_n$ groups in $LiPF_6$/PEO (cutoff distance 5 Å).

Table 4
$LiPF_6$/PPGDA viscoelastic properties vs $LiPF_6$ concentration.

Li:EO[a]	C [mol/l]	ρ [g/cm^3]	E [GPa], $\varepsilon_{avg}=0.07$, $d\varepsilon/dt=0.8\ ns^{-1}$	E [GPa], $\varepsilon_{avg}=0.03$, $d\varepsilon/dt=0.08\ ns^{-1}$	η_{NEMD} [mPa·s] [29]	η[a] [mPa·s]
0	0	1.167	0.88 ± 0.02	0.78 ± 0.02	15.8 ± 4.0	118 ± 29
1:32	0.48	1.152	0.51 ± 0.01	0.69 ± 0.03	9.6 ± 2.7	124 ± 40
1:16	0.92	1.152	0.57 ± 0.02	1.26 ± 0.03	9.7 ± 3.3	608 ± 96

[a] Einstein/Green-Kubo relations

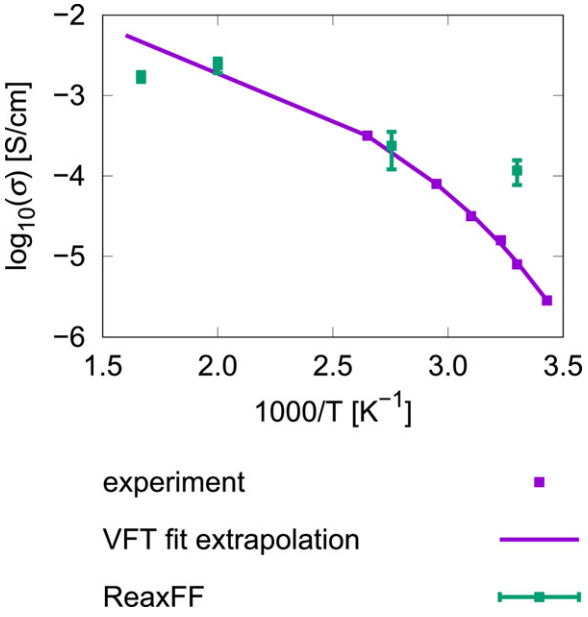

Fig. 8. $LiPF_6$/PEO ionic conductivity vs inverse temperature (experimantal data from [61]).

due to $LiPF_6$. From Li-P distributions (Fig. 10b), an increase in coordination w.r.t. the first and second coordination shells (indicated by the first and second RDF maxima, resp.) due to increasing $LiPF_6$ concentration was found. Based on it, larger $Li(PF_6)_n$ cluster sizes were assumed. The conclusion was supported by the obtained Li-$(PF_6)_n$ group distributions (Fig. 12), which indicate a significant proportion of dissociated salt molecules and smaller proportions of $Li(PF_6)_1$ and $Li(PF_6)_2$ for the lowest $LiPF_6$ concentration. The presence of $Li(PF_6)_3$ groups in the lower concentration structure without analogous groups being observed in the higher concentration structure was attributed to the statistical limitation due to relatively small number of salt molecules considered (12 and 24, resp.). In contrast, a small reduction in the P-P and Li-O first neighbor coordination at increasing $LiPF_6$ concentration was observed (Fig. 10a,c). Subsequently, considering that at the simulation temperature $LiPF_6$ represents a solid phase material with a significantly higher density (T_m = 467K, ρ = 2.838 g/cm^3 [64]), we could conclude that the stiffening of the material's response was a result of $LiPF_6$ concentration dependent component segregation. Moreover, distinct increase in shear stress relaxation modulus anisotropy (Fig. 11) suggests that the $LiPF_6$ concentration may enhance local anisotropy of the material's viscoelastic properties.

Further, we would like to highlight the qualitative dependence of the material's response on deformation strain rate and equilibrium conditions by comparing the results above to the same quantities at strictly non-equilibrium conditions. The conditions include approximately two times higher reference strain (mean value 0.07) and an order higher strain rate (0.8 ns^{-1}) for dynamic stiffness calculation and shear viscosity estimation using a momentum exchange approach [29]. The comparison was intended as an attempt to link the aforementioned simulation conditions to relevant material states. The results (Table 4) indicate a nonlinear reduction of both quantities due to $LiPF_6$ concentration. Due to higher mean reference strain ($LiPF_6$ concentration dependent) for the 0.8 ns^{-1} strain rate, the obtained moduli values were considered to represent a material response that involves significantly higher deformation state compared to the moduli at 0.08 ns^{-1} strain rate. Likewise, since the non-equilibrium shear viscosity indicates one or two orders of magnitude reduction w.r.t. the equilibrated structures, it was assumed to represent phenomena that are applicable to strictly non-equilibrium conditions, e.g., rapid temperature change. Moreover, since this order of magnitude corresponds to that of noncrosslinked structure's equilibrium viscosity (9.7 ± 1.2 mPa·s), we suggest that the full crosslink effect on the material's viscoelastic properties necessitates equilibration/loading timescales which are compatible with the relaxation timescale of material. Subsequently, the observed differences in material response should be considered for higher length scale computational material models under analogous loading conditions.

3.4. $LiPF_6$ concentration effects on material failure

The failure simulation results (Tables 5 and 6) indicate that increasing $LiPF_6$ concentration reduces material strength and failure strain. It is observed that the number of dissociated bond counts during deformation decreases significantly with $LiPF_6$ concentration for the triaxial tension loading and slightly increases for the simple shear loading. The latter difference, which characterizes

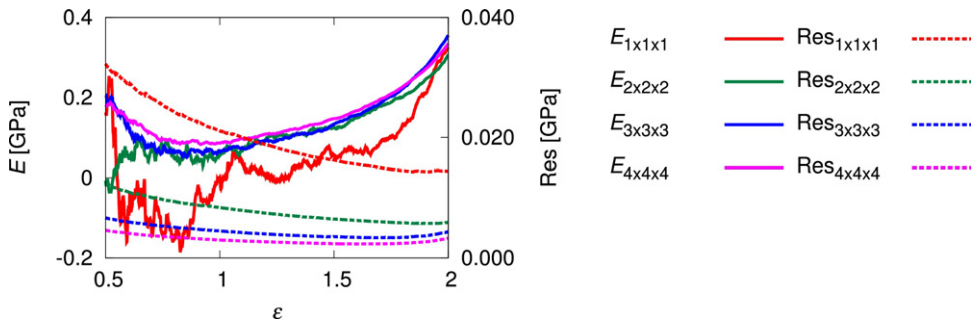

Fig. 9. Comparison of PPGDA dynamic stiffness (E), and normalized curve fit residual (Res) vs reference strain for different system sizes/unit cell expansions ($d\varepsilon/dt = 8\ ns^{-1}$) at 300K.

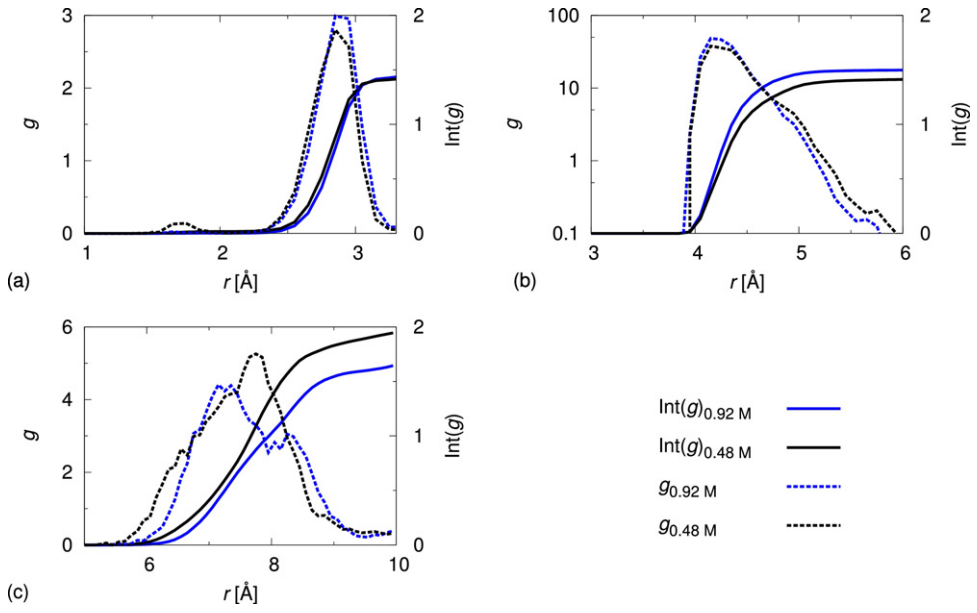

Fig. 10. $LiPF_6$ concentration dependent (a) Li-O, (b) Li-P, and (c) P-P radial distributions in $LiPF_6$/PPGDA.

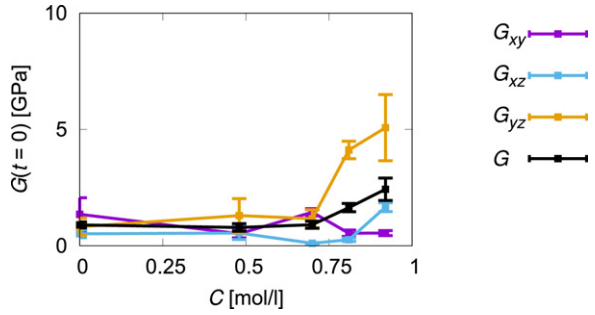

Fig. 11. $LiPF_6$ concentration dependence of $LiPF_6$/PPGDA initial shear stress relaxation modulus $G(t=0)$.

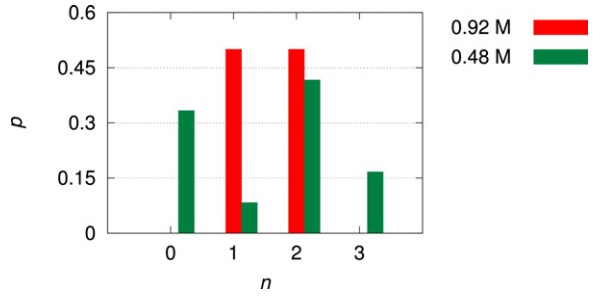

Fig. 12. $LiPF_6$ concentration dependent $Li(PF_6)_n$ group distributions in $LiPF_6$/PPGDA (cutoff distance 5 Å).

the extent of material damage at failure, is ascribed to intrinsic differences due to volume preserving and non-preserving deformations. Further, the dissociation of all C—O acrylate-ethylene bonds (128 in total) for the expansion deformation and all dissociating bonds belonging to the aforementioned bond type for the simple shear deformation indicate that primarily these bonds are likely to account for the initiation of material failure. As discussed above (Section 3.1), this behavior is in agreement with the estimated bond dissociation energy predictions. In contrast, no bond dissociation failure up to 10 GPa in hydrostatic compression was detected.

Table 5
Bond dissociation statistics and failure pressure/density values for triaxial tension of $LiPF_6$/PPGDA and PPGDA ($n_{C\text{-}O}$ = broken C-O bonds, $n_{C\text{-}C}$ = broken C-C bonds, P_f = failure pressure, $\Delta V_f/V$ = volumetric strain at failure).

Li:EO	$n_{C\text{-}O}$	$n_{C\text{-}C}$	P_f [GPa]	$\Delta V_f/V$
0	256	61	-0.232 ± 0.005	10.3
1:32	126	0	-0.231 ± 0.004	9.9
1:16	159	0	-0.20 ± 0.01	9.0

Table 6
Bond dissociation statistics and failure pressure/strain values for simple shear deformation of $LiPF_6$/PPGDA and PPGDA ($n_{C\text{-}O}$ = broken C-O bonds, $n_{C\text{-}C}$ = broken C-C bonds, τ_f = failure stress, ε_f = failure strain).

Li:EO	$n_{C\text{-}O}$	$n_{C\text{-}C}$	τ_f [GPa]	ε_f
0	16	0	1.5	3.0
1:32	20	0	1.2	2.8
1:16	22	0	1.1	2.7

4. Summary and conclusions

An agreement with experimental results on similar materials has been found regarding a correlation between material's stiffness and electrolyte salt concentration. The observed behavior has been explained in the context of material nanoscale structure, considering radial distributions, and microscale structure, considering the effect of ion clustering on the material's viscosity. Further, in agreement with bond dissociation statistics, the triaxial tensile and simple shear deformation simulations indicate reduced material strength and failure strain at increasing $LiPF_6$ concentrations. Subsequently, the results facilitate the assessment of correlations between mechanical and electrochemical properties of a crosslinked PPGDA/$LiPF_6$ electrolyte. Complementarily, the implications of uniaxial loading strain and fast thermal fluctuations on material's mechanical response, resulting in significantly reduced stiffness and viscosity, respectively, have been discussed.

In similarity with $LiPF_6$ solvation structures in $LiPF_6$/PEO based SPE, an opportunity for improvement w.r.t. salt ion dissociation and solvation properties has been identified. For the achievement of the latter objective, alternative salts and plasticizers [65,56] (see also Section 1) could be considered.

Acknowledgements

The research leading to these results has received funding from the European Research Council under the European Union's Seventh Framework Programme (FP7/2007-2013) / ERC Grant agreement n° 617972.

The VASP/DDEC calculation of $LiPF_6$ ion dissociation energy and charges by Dr. Seung Geol Lee (Department of Organic Material Science and Engineering, Pusan National University, Republic of Korea) is gratefully acknowledged.

References

[1] B. Sun, D. Rehnlund, M.J. Lacey, D. Brandell, Electrodeposition of thin poly(propylene glycol) acrylate electrolytes on 3D-nanopillar electrodes, Electrochimica Acta 137 (0) (2014) 320–327, URL http://www.sciencedirect.com/science/article/pii/S001346861401189X.

[2] E.L. Wong, D.M. Baechle, K. Xu, R.H. Carter, J.F. Snyder, E.D. Wetzel, Design and processing of structural composite batteries, International SAMPE Symposium and Exhibition (Proceedings) 52 (2007), URL http:// www.scopus. com/ inward/ record. url?eid=2- s2. 0-34748865393&partnerID=40&md5=983cf8a23f55a4bbf9e42fed7649c268.

[3] M. Willgert, M.H. Kjell, E. Jacques, M. Behm, G. Lindbergh, M. Johansson, Photoinduced free radical polymerization of thermoset lithium battery electrolytes, European Polymer Journal 47 (12) (2011) 2372–2378, URL http://www.sciencedirect.com/science/article/pii/S0014305711003491.

[4] L.E. Asp, E.S. Greenhalgh, Structural power composites, Composites Science and Technology 101 (2014) 41–61, URL http:// www. scopus. com/ inward/ record. url?eid=2- s2. 0-84904497074&partnerID=40&md5=e3e33beee59e9c35b839e9a4ecf17a22.

[5] F. Gasco, P. Feraboli, Manufacturability of composite laminates with integrated thin film Li-ion batteries, Journal of Composite Materials 48 (8) (2014) 899–910, URL http://jcm.sagepub.com/content/48/8/899.abstract.

[6] S. Leijonmarck, T. Carlson, G. Lindbergh, L.E. Asp, H. Maples, A. Bismarck, Solid polymer electrolyte-coated carbon fibres for structural and novel micro batteries, Composites Science and Technology 89 (2013) 149–157, URL http://www.scopus.com/inward/record.url?eid=2-s2.0-84887014038&partnerID=40&md5=4e85764855fc39c30df2a4a49e73bc26.

[7] M. Willgert, M.H. Kjell, G. Lindbergh, M. Johansson, New structural lithium battery electrolytes using thiol-ene chemistry, Solid State Ionics 236 (2013) 22–29, URL http://www.sciencedirect.com/science/article/pii/S016727381300091X.

[8] J.K. Park, Principles and Applications of Lithium Secondary Batteries, Wiley, 2012, URL http://www.scopus.com/inward/record.url?eid=2-s2.0-84891579865&partnerID=40&md5=846b4ecc561c7bb0101eaaa9e8d30a39.

[9] L.E. Asp, S. Leijonmarck, T. Carlson, G. Lindbergh, Realisation of structural battery composite materials, in: 20th International Conference on Composite Materials (Proceedings), 2015, URL http://www.iccm20.org/1121-2.

[10] N.S. Ergang, M.A. Fierke, Z. Wang, W.H. Smyrl, A. Stein, Fabrication of a fully infiltrated three-dimensional solid-state interpenetrating electrochemical cell, Journal of the Electrochemical Society 154 (12) (2007) A1135–A1139, URL http://www.scopus.com/inward/record.url?eid=2-s2.0-35549004013&partnerID=40&md5=ad1ca103b1bd3a8e6bc9f578c1c629de.

[11] B. Dunn, J.W. Long, D.R. Rolison, Rethinking multifunction in three dimensions for miniaturizing electrical energy storage, Electrochemical Society Interface 17 (3) (2008) 49–53, URL http://www.scopus.com/inward/record.url?eid=2-s2.0-70350434840&partnerID=40&md5=044938757f3a09b8ec4b9ec9099ba17a.

[12] C.H. San, C.W. Hong, Molecular design of the solid copolymer electrolyte-poly(styrene-b-ethylene oxide) for lithium ion batteries, Computers, Materials and Continua 23 (2) (2011) 101–117, URL http:// www.scopus. com/ inward/ record. url?eid=2- s2. 0-80051697359&partnerID=40&md5=b230cfba7a971cc2e3826e40db7220c5.

[13] E.D. Gomez, A. Panday, E.H. Feng, V. Chen, G.M. Stone, A.M. Minor, C. Kisielowski, K.H. Downing, O. Borodin, G.D. Smith, N.P. Balsara, Effect of ion distribution on conductivity of block copolymer electrolytes, Nano Letters 9 (3) (2009) 1212–1216, URL http://dx.doi.org/10.1021/nl900091n.

[14] M. Grujicic, K.M. Chittajallu, G. Cao, W.N. Roy, An atomic level analysis of conductivity and strength in poly(ethylene oxide) sulfonic acid-based solid polymer electrolytes, Materials Science and Engineering: B 117 (2) (2005) 187–197, URL http://www.sciencedirect.com/science/article/pii/S0921510704006166.

[15] A.S. Westover, F.N. Shabab, J.W. Tian, S. Bernath, L. Oakes, W.R. Erwin, R. Carter, R. Bardhan, C.L. Pint, Stretching ion conducting polymer electrolytes: In-situ correlation of mechanical, ionic transport, and optical properties, Journal of The Electrochemical Society 161 (6) (2014) E112–E117, URL http://jes.ecsdl.org/content/161/6/E112.abstract.

[16] M. Willgert, M.H. Kjell, M. Johansson, Effect of lithium salt content on the performance of thermoset lithium battery electrolytes, ACS Symposium Series 1096 (2012) 55–65, URL http://www.scopus.com/inward/record.url?eid=2-s2.0-84905577275&partnerID=40&md5=faa4fcf31273401b3b55624ee8775ba6.

[17] T. Kelly, B.M. Ghadi, S. Berg, H. Ardebili, In situ study of strain-dependent ion conductivity of stretchable polyethylene oxide electrolyte, Scientific reports 6 (2016).

[18] G. Schaftenaar, J.H. Noordik, Molden: A pre- and post-processing program for molecular and electronic structures, Journal of Computer-Aided Molecular Design 14 (2) (2000) 123–134.

[19] S. Plimpton, Fast parallel algorithms for short-range molecular dynamics, Journal of Computational Physics 117 (1) (1995) 1–19, URL http://www.sciencedirect.com/science/article/pii/S002199918571039X.

[20] H.M. Aktulga, J.C. Fogarty, S.A. Pandit, A.Y. Grama, Parallel reactive molecular dynamics: Numerical methods and algorithmic techniques, Parallel Computing 38 (4-5) (2012) 245–259, URL http://dx.doi.org/10.1016/j.parco.2011.08.005.

[21] C. Svaneborg, G.S. Grest, R. Everaers, Disorder effects on the strain response of model polymer networks, Polymer 46 (12) (2005) 4283–4295, in Honor of James E. Mark. URL http://www.sciencedirect.com/science/article/pii/S0032386105002727.

[22] A.C.T. van Duin, S. Dasgupta, F. Lorant, W.A. Goddard III, ReaxFF: A reactive force field for hydrocarbons, The Journal of Physical Chemistry A 105 (41) (2001) 9396–9409, URL http://dx.doi.org/10.1021/jp004368u.

[23] A.K. Rappe, W.A. Goddard III, Charge equilibration for molecular dynamics simulations, The Journal of Physical Chemistry 95 (8) (1991) 3358–3363, URL http://dx.doi.org/10.1021/j100161a070.

[24] M.M. Islam, V.S. Bryantsev, A.C.T. van Duin, ReaxFF reactive force field simulations on the influence of teflon on electrolyte decomposition during Li/SWCNT anode discharge in lithium-sulfur batteries, Journal of the Electrochemical Society 161 (8) (2014) E3009–E3014, URL http:// www.scopus. com/ inward/ record. url?eid=2- s2. 0-84904809777&partnerID=40&md5=74af8f84175099e1b0060df7b61ae6ed.

[25] M.T. Ong, O. Verners, E.W. Draeger, A.C.T. van Duin, V. Lordi, J.E. Pask, Lithium ion solvation and diffusion in bulk organic electrolytes from first-principles and classical reactive molecular dynamics, The Journal of Physical Chemistry B 119 (4) (2015) 1535–1545, URL http://dx.doi.org/10.1021/jp508184f.

[26] *LAMMPS documentation*, http://lammps.sandia.gov/doc/Manual.html, accessed 2015-03-15 (2015).

[27] M.E. Tuckerman, J. Alejandre, R. Lopez-Rendonn, A.L. Jochim, G.J. Martyna, A Liouville-operator derived measure-preserving integrator for molecular dynamics simulations in the isothermal-isobaric ensemble, Journal of Physics A: Mathematical and General 39 (19) (2006) 5629, URL http://stacks.iop.org/0305-4470/39/i=19/a=S18.

[28] W. Shinoda, M. Shiga, M. Mikami, Rapid estimation of elastic constants by molecular dynamics simulation under constant stress, Physical Review B 69 (2004) 134103, URL http://link.aps.org/doi/10.1103/PhysRevB.69.134103.

[29] F. Müller-Plathe, Reversing the perturbation in nonequilibrium molecular dynamics: An easy way to calculate the shear viscosity of fluids, Physical Review E 59 (1999) 4894–4898, URL http://link.aps.org/doi/10.1103/PhysRevE.59.4894.

[30] G. Kresse, J. Hafner, *Ab initio* molecular dynamics for liquid metals, Physical Review B 47 (1993) 558–561, URL http://link.aps.org/doi/10.1103/PhysRevB.47.558.

[31] G. Kresse, J. Furthmüller, Efficient iterative schemes for *ab initio* total-energy calculations using a plane-wave basis set, Physical Review B 54 (1996) 11169–11186, URL http://link.aps.org/doi/10.1103/PhysRevB.54.11169.

[32] P.E. Blöchl, Projector augmented-wave method, Physical Review B 50 (1994) 17953–17979, URL http://link.aps.org/doi/10.1103/PhysRevB.50.17953.

[33] G. Kresse, D. Joubert, From ultrasoft pseudopotentials to the projector augmented-wave method, Physical Review B 59 (1999) 1758–1775, URL http://link.aps.org/doi/10.1103/PhysRevB.59.1758.

[34] J.P. Perdew, K. Burke, M. Ernzerhof, Generalized gradient approximation made simple, Physical Review Letters 77 (1996) 3865–3868, URL http://link.aps.org/doi/10.1103/PhysRevLett.77.3865.

[35] S. Grimme, S. Ehrlich, L. Goerigk, Effect of the damping function in dispersion corrected density functional theory, Journal of Computational Chemistry 32 (7) (2011) 1456–1465, URL http://dx.doi.org/10.1002/jcc.21759.

[36] S. Wilson, G.H.F. Diercksen, Methods in Computational Molecular Physics, Nato Science Series B. Springer, 2013.

[37] P. Pulay, Convergence acceleration of iterative sequences, The case of SCF iteration, Chemical Physics Letters 73 (2) (1980) 393–398, URL http://www.sciencedirect.com/science/article/pii/0009261480803964.

[38] G. Kresse, M. Marsman, J. Furthmüller, VASP documentation (2015), http://cms.mpi.univie.ac.at/vasp/vasp/vasp.htmlhttp://cms.mpi.univie.ac.at/vasp/vasp/vasp.html, accessed 2015-05-24.

[39] P.E. Blöchl, O. Jepsen, O.K. Andersen, Improved tetrahedron method for Brillouin-zone integrations, Physical Review B 49 (1994) 16223–16233, URL http://link.aps.org/doi/10.1103/PhysRevB.49.16223.

[40] A. De Vita, M.J. Gillan, The energetics of hydrogen in aluminium calculated from first principles, Journal of Physics: Condensed Matter 4 (2) (1992) 599, URL http://stacks.iop.org/0953-8984/4/i=2/a=028.

[41] H.J. Monkhorst, J.D. Pack, Special points for Brillouin-zone integrations, Physical Review B 13 (1976) 5188–5192, URL http://link.aps.org/doi/10.1103/PhysRevB.13.5188.

[42] T.A. Manz, D.S. Sholl, Improved atoms-in-molecule charge partitioning functional for simultaneously reproducing the electrostatic potential and chemical states in periodic and nonperiodic materials, Journal of Chemical Theory and Computation 8 (8) (2012) 2844–2867.

[43] D. Frenkel, B. Smit, Understanding molecular simulation: From algorithms to applications, Academic Press, 1996, URL http:// www. scopus. com/ inward/ record. url?eid=2- s2. 0-84870726202&partnerID=40&md5=de31eed96d6714750e143c551692fdef.

[44] M.P. Allen, D.J. Tildesley, Computer Simulation of Liquids, Oxford University Press, 1989.
[45] F. Müller-Plathe, Permeation of polymers – a computational approach, Acta Polymerica 45 (4) (1994) 259–293, URL http://dx.doi.org/10.1002/actp.1994.010450401.
[46] B. Hess, Determining the shear viscosity of model liquids from molecular dynamics simulations, The Journal of Chemical Physics 116 (1) (2002) 209–217, URL http://scitation.aip.org/content/aip/journal/jcp/116/1/10.1063/1.1421362.
[47] G.D. Smith, D. Bedrov, L. Li, O. Byutner, A molecular dynamics simulation study of the viscoelastic properties of polymer nanocomposites, The Journal of Chemical Physics 117 (20) (2002) 9478–9489, URL http://scitation.aip.org/content/aip/journal/jcp/117/20/10.1063/1.1516589.
[48] B. Hong, F. Escobedo, A.Z. Panagiotopoulos, Diffusivities and viscosities of poly(ethylene oxide) oligomers, Journal of Chemical & Engineering Data 55 (10) (2010) 4273–4280, URL http://dx.doi.org/10.1021/je100430q.
[49] C.M. Tenney, E.J. Maginn, Limitations and recommendations for the calculation of shear viscosity using reverse nonequilibrium molecular dynamics, The Journal of Chemical Physics 132 (1) (2010) 014103, URL http://scitation.aip.org/content/aip/journal/jcp/132/1/10.1063/1.3276454.
[50] R.D. Raharjo, H. Lin, D.F. Sanders, B.D. Freeman, S. Kalakkunnath, D.S. Kalika, Relation between network structure and gas transport in crosslinked poly(propylene glycol diacrylate), Journal of Membrane Science 283 (1-2) (2006) 253–265, URL http://www.sciencedirect.com/science/article/pii/S0376738806004248.
[51] A. Stukowski, Visualization and analysis of atomistic simulation data with OVITO the open visualization tool, Modelling and Simulation in Materials Science and Engineering 18 (1) (2010) 015012, URL http://stacks.iop.org/0965-0393/18/i=1/a=015012.
[52] Sigma-Aldrich Co. LLC, *Online product catalog*, http://www.sigmaaldrich.com/technical-service-home/product-catalog.html, accessed 2015-3-20 (2015).
[53] O. Borodin, G.D. Smith, R.L. Jaffe, Ab initio quantum chemistry and molecular dynamics simulations studies of LiPF6/poly(ethylene oxide) interactions, Journal of Computational Chemistry 22 (6) (2001) 641–654, URL http://dx.doi.org/10.1002/jcc.1033.
[54] J. Karo, D. Brandell, A molecular dynamics study of the influence of side-chain length and spacing on lithium mobility in non-crystalline LiPF6PEOx; x=10 and 30, Solid State Ionics 180 (2325) (2009) 1272–1284, URL http://www.sciencedirect.com/science/article/pii/S0167273809002793.
[55] A. Maitra, A. Heuer, Cation transport in polymer electrolytes: A microscopic approach, Physical Review Letters 98 (22) (2007) 227802, URL http:// www.scopus. com/ inward/ record. url?eid=2- s2. 0-34547377300&partnerID=40&md5=6b4c4f7b9b1c1b7a4f9de05da0a591dc.
[56] H. Wu, C.D. Wick, Computational investigation on the role of plasticizers on ion conductivity in poly(ethylene oxide) LiTFSI electrolytes, Macromolecules 43 (7) (2010) 3502–3510, URL http://www.scopus.com/inward/record.url?eid=2-s2.0-77951528059&partnerID=40&md5=05a20ae1eb04e3f44a8f0017d4820f20.
[57] M.K. Beyer, The mechanical strength of a covalent bond calculated by density functional theory, The Journal of Chemical Physics 112 (17) (2000) 7307–7312, URL http://scitation.aip.org/content/aip/journal/jcp/112/17/10.1063/1.481330.
[58] S.J. Blanksby, G.B. Ellison, Bond dissociation energies of organic molecules, Accounts of Chemical Research 36 (4) (2003) 255–263, URL http://dx.doi.org/10.1021/ar020230d.
[59] E. Bitzek, P. Koskinen, F. Gähler, M. Moseler, P. Gumbsch, Structural relaxation made simple, Physical Review Letters 97 (2006) 170201, URL http://link.aps.org/doi/10.1103/PhysRevLett.97.170201.
[60] F. Han, J. Zhang, G. Chen, X. Wei, Density, viscosity, and excess properties for aqueous poly(ethylene glycol) solutions from (298.15 to 323.15) K, Journal of Chemical & Engineering Data 53 (11) (2008) 2598–2601, URL http://dx.doi.org/10.1021/je800464t.
[61] S. Arumugam, J. Shi, D.P. Tunstall, C.A. Vincent, Cation and anion diffusion coefficients in a solid polymer electrolyte measured by pulsed-field-gradient nuclear magnetic resonance, Journal of Physics: Condensed Matter 5 (2) (1993) 153.
[62] N.P. Patel, C.M. Aberg, A.M. Sanchez, M.D. Capracotta, J.D. Martin, R.J. Spontak, Morphological, mechanical and gas-transport characteristics of crosslinked poly(propylene glycol): Homopolymers, nanocomposites and blends, Polymer 45 (17) (2004) 5941–5950, URL http://www.sciencedirect.com/science/article/pii/S0032386104006093.
[63] C. Lefrou, P. Fabry, J.C. Poignet, Electrochemistry: The Basics, with Examples, Springer-Verlag, 2012.
[64] E. Zinigrad, L. Larush-Asraf, J.S. Gnanaraj, M. Sprecher, D. Aurbach, On the thermal stability of LiPF6, Thermochimica Acta 438 (12) (2005) 184–191, URL http://www.sciencedirect.com/science/article/pii/S0040603105004879.
[65] Y.T. Kim, E.S. Smotkin, The effect of plasticizers on transport and electrochemical properties of PEO-based electrolytes for lithium rechargeable batteries, Solid State Ionics 149 (12) (2002) 29–37, URL http://www.sciencedirect.com/science/article/pii/S0167273802001303.